Available online at www.sciencedirect.com

ScienceDirect

Procedia Materials Science 6 (2014) 557 – 566

Procedia Materials Science

www.elsevier.com/locate/procedia

3rd International Conference on Materials Processing and Characterization (ICMPC 2014)

Effect of Ag doping on Antibacterial and Photocatalytic Activity of Nanocrystalline TiO_2

M. Harikishore[a,b], M. Sandhyarani[a,*], K. Venkateswarlu[a,c], T.A. Nellaippan[a], N. Rameshbabu[a]

[a]*Department of Metallurgical and Materials Engineering, National Institute of Technology, Tiruchirappalli 620015, Tamilnadu, India*
[b]*Sievert India Private Limited, Nerul, Navi Mumbai, Mumbai 400706, Maharastra, India*
[c]*Department of Physics, National Institute of Technology, Tiruchirappalli 620015, Tamilnadu, India*

Abstract

In the present study, nanocrystalline pure TiO_2 and 5 mol% silver doped TiO_2 (Ag-TiO_2) powders were prepared by sol-gel route. The prepared powders were characterized by X-ray diffraction (XRD) and UV-Visible spectroscopy (UV-Vis) for their phase composition and optical properties, respectively. The antibacterial property of TiO_2 and Ag-TiO_2 was assessed by spread plate method against *Escherichia coli* as test bacteria. The photocatalytic activity of Ag-TiO_2 was studied by measuring degradation of Methylene blue (MB) under UV Irradiation and the results were compared with pure TiO_2. Further, the effect of temperature and dye concentration on degradation efficiency of pure TiO_2 was studied. XRD results confirm the presence of anatase phase in both the samples and the average crystallite size of both samples were found in the order of 6-15 nm. Addition of Ag reduces the band gap of TiO_2 from 3.1 eV to 2.9 eV. In 24 h of incubation period, Ag-TiO_2 showed complete inhibition of growth of *Escherichia coli* compared to pure TiO_2. It was observed that the degradation efficiency was more for TiO_2 annealed at 500 ˚C compared to as-synthesis TiO_2 and it decreases with further increase in temperature. In addition, as the dye concentration increases, the degradation efficiency of pure TiO_2 decreases. Among, TiO_2 and Ag-TiO_2 samples, MB degradation efficiency was higher for Ag-TiO_2 compared to pure TiO_2. Photo degradation of MB was modeled with power law kinetics and was observed to follow first order kinetics and the rate constant was enhanced with Ag doping in TiO_2.

Selection and peer review under responsibility of the Gokaraju Rangaraju Institute of Engineering and Technology (GRIET)

Keywords: Titanium dioxide; silver; sol-gel process; antibacterial property; photocatalytic activity; power-law kinetics.

* Corresponding author.. Tel.: +0-431-250-3471; fax: +0-431-250-0133.
E-mail address: sandhyarani.muthyala@gmail.com

Selection and peer review under responsibility of the Gokaraju Rangaraju Institute of Engineering and Technology (GRIET)
doi:10.1016/j.mspro.2014.07.071

1. Introduction

Nanostructured and nanophasic materials have been extensively studied because of their unique properties which extends the spectrum of their applications in different fields. The impact of nanostructure on the properties of high surface area materials is an area of increasing importance for understanding, creating and improving materials in diverse applications (Koch, 2006). The study of nanometer size semiconductor crystals has been gaining much interest because, the physical and chemical properties of these semiconductor crystals can be systematically tuned by variation of the size according to increasingly well established scaling laws (Wilson et al., 2002). Among the various classes of materials, metal oxides are the most common, diverse and probably the richest class of materials in terms of physical, chemical and structural properties. Further, oxide nanoparticles can exhibit unique physical and chemical properties due to their small size and a higher number of surface atoms (Rodriguez and Fernandez, 2007).

Nanocrystalline titania (TiO_2) becomes increasingly important because of its potential application in catalysis/photocatalysis, coatings on self-cleaning surfaces, photovoltaic applications and removal of heavy metal ions from solutions for detoxification and oxidation of toxic organic contaminants in water to carbon dioxide, ceramic membranes and gas sensors (Fujishima and Zhang, 2006; Diebold, 2003). The wide range of applications of TiO_2 is mainly due to its properties like chemical inertness, non-toxicity and stability over a wide range of pH under irradiation conditions (Sharad et al., 2012; Fujishima et al., 2000). However, its band gap is so large (E_g = 3.20 eV) to be only excited under UV light with a wavelength less than 387.5 nm, which accounts for only 5% of the incoming solar energy (Dulce et al., 2013; Chen and Mao, 2007). Therefore, current research interests in shifting the absorption spectrum of TiO_2 towards the visible region in order to take the full advantage of sun light. In addition, a low rate of electron transfer to oxygen and a high recombination of photo generated electron-hole pair results low quantum efficiency (Diwald et al., 2004; Carp et al., 2004). Thus, to improve the response of TiO_2 to visible light and to enhance the separation of electron hole pairs, numerous methods including transition metal (Mukhtar et al., 2011; Wilke and Breuer, 1999), rare-earth metal (Ramya et al., 2013) and non metal (Nosaka et al., 2005) doped TiO_2 have been synthesized.

Silver (Ag) has been known to exhibit strong cytotoxicity towards a broad range of micro-organisms. Ag ions are capable of causing bacteriostatic or even bactericidal impact (Mukhtar et al., 2011; Morones et al., 2005). This bactericidal behavior of Ag nanoparticles is attributed to the presence of electronic effects, which is a result of the changes in the local electronic structure on the surfaces of smaller-sized particles. These effects are considered to be contributing towards an enhancement of the reactivity of Ag nanoparticle surfaces (Maness et al., 1999). It was reported that ionic Ag strongly interacts with thiol group of vital enzymes and inactivates them (Feng et al., 2000). Ag doping in TiO_2 is expected to show various effects on its photocatalytic activity by the following mechanisms. It may (i) enhance the electron-hole separation by acting as electron traps, (ii) extend the light absorption into the visible range and enhance surface electron excitation by Plasmon resonances excited by visible light and (iii) modify the surface properties of photo catalysts (Seery et al., 2007). Potential application for photocatalytic Ag doped TiO_2 include self-cleaning surfaces for water purification. He et al. (2002) investigated the effect of Ag doping on the photocatalytic activity of the TiO_2 films. They reported that the increase in photocatalytic activity by doping Ag into TiO_2 is due to the increase in interfacial charge transfer efficiency for TiO_2 and due to enhancement in the charge pair separation and thereby inhibiting their recombination.

A number of methods have been used to prepare TiO_2 nanopowders, such as co-precipitation (Quan et al., 2007), mechanochemical (Yin et al., 2003), hydrothermal (Wang, 2007) and sol-gel (Mohammadi et al., 2008) synthesis. From the last few decades, the sol-gel process has become one of the successful techniques for preparing nanocrystalline metallic oxide materials. The homogeneous properties of the products prepared by this method are very satisfactory (Ding and Liu, 1997). A unique property of sol-gel process is an ability to go all the way from molecular precursor to the product, allowing a better control of the whole process and the synthesis of tailor made materials for various applications (Brinker and Scherrer, 1990). In this paper, nanosized TiO_2 and Ag-TiO_2 powders are prepared by sol-gel process. The physical properties of the prepared powders are characterized by UV-Vis spectroscopy and XRD. The influence of the irradiated photo catalyst TiO_2 and Ag-TiO_2 on degradation of

Methylene Blue (MB, $C_{16}H_{18}N_3S$) in aqueous system is studied. Since *Escherichia coli* had been used as a biological indicator of water system, it is taken as a model in our work for antibacterial studies.

2. Experimental

2.1. Materials

Titanium tetra n-butoxide (E. Merck, Germany) was used as titanium precursor and silver nitrate (E. Merck, Germany) was taken as Ag precursor. Titanium tetra n-butoxide was taken as titanium precursor because of its lower reactivity with atmosphere compared to other titanium source precursors like titanium isopropoxide and titanium tetra chloride. A catalyst was used to control hydrolysis and condensation reactions. Acetic acid and double distilled water were used as reagents in the present study.

2.2. Synthesis of TiO_2 powders

5 ml of titanium tetra n-butoxide was dissolved in 8.5 ml of acetic acid. 26.6 ml of double distilled water was added drop wise to this mixture under constant stirring conditions. Titanium tetra n-butoxide, acetic acid and water are maintained in the molar ratio of 1:10:100. The solution was stirred for 8 h to get a clear transparent sol and allowed to dry at 100 ˚C after which it was annealed to specified temperature in air for 5 h. To prepare Ag doped TiO_2, the silver nitrate (5 mol%, 0.124 g) was added to the water and the above procedure was repeated.

2.3 Characterization

Powder XRD was used for identification of crystalline phases and for estimation of crystallite size. The XRD patterns were recorded in 2θ range of 20˚ to 80˚ by step scanning with 2θ increment of 0.05 and a scan speed of 1˚/min employing Cu K_α radiation with wavelength of 0.15406 nm (Ultima-III, Rigaku, Japan). The average crystallite size of the samples was determined using Scherer's equation (Klug and Alexander, 1954) considering full width at half maximum (FWHM) for the (101) diffraction peak of anatase phase as;

$$d = \frac{0.9\lambda}{\beta \cos\theta} \tag{1}$$

where, d is average crystallite size in nm, 0.9 is Scherrer constant, λ is wavelength of the X-ray (0.154 nm for Cu K_α radiation), θ is Bragg's diffraction angle (˚) and β is broadening of the diffraction peak measured at half of its maximum intensity (FWHM in radians). Crystallite size 'd' and lattice strain 'ε' of anatase phase were separately determined from sinθ dependence of FWHM intensity β of the diffraction lines, according to the Williamson-Hall equation (Venkateswarlu et al., 2010);

$$\beta \cos\theta = \left(\frac{k\lambda}{d} \right) + 2\varepsilon \sin\theta \tag{2}$$

where, λ is the wavelength of Cu K_α radiation (0.154 nm). From the plots of βcosθ against sinθ for the sample, crystallite size 'd' is calculated from the intercept of the linear extrapolation and lattice strain 'ε' is determined from its slope. Details of determination of 'd' and 'ε' were reported in elsewhere (Klug and Alexander, 1954). The UV-Vis absorbance spectrum for the samples is recorded using Shimadzu (UV-1700) UV-Vis spectrophotometer. The measurement was taken in a wavelength range of 200-800 nm. The band gap energy (E_g) can be estimated by the conventional Tauc equation (Peiqiang et al., 2014).

2.4 Antibacterial studies

Antibacterial activity of pure TiO_2 and Ag-TiO_2 was examined by spread plate method (Sandhyarani et al., 2013). Gram negative *Escherichia coli* bacteria were used as model bacteria for the present study. Gram is the most familiar and renowned categorization of bacteria's, they can be either Gram positive or negative depending on the

composition of the bacteria cellular membrane (Gonzalez et al., 2012). Nutrient agar was used as source for culturing bacteria. 1 mg of each sample was mixed individually with 1 mL of phosphate buffer solution (pH 7.4) containing 1×10^5 cells/mL *Escherichia coli* in flat-bottom test tubes. Each tube was shaken at 200 rpm at 30 ˚C for 24 h. 100 µL of shaken solutions were placed into Petri plates in duplicate and a nutrient medium agar was overlaid onto the inoculum, spread evenly in clockwise-anticlockwise directions and left undisturbed for the agar to solidify. After solidification, these plates were incubated at 37 ˚C for 24 h. The colony formation was examined and photographed.

2.5 Photocatalytic activity

In order to evaluate photocatalytic activity of the samples, decomposition behavior of MB in water was studied. 100 mL of 5 x 10^{-5} M concentration of MB was added to 0.15 g/L of sample and was dispersed under ultrasonic vibration for 5 min. The solution was kept in dark for 30 min under stirring to saturate the adsorption of MB into each sample and then the solution was irradiated under UV light. For UV irradiation, a UV lamp of 400 W was used at the distance of about 150 mm from the solution. MB degradation was monitored by collecting aliquots at increasing and equal time intervals. The aliquots were centrifuged and absorption spectra were recorded using UV-Vis spectrophotometer (UV-1700, Shimadzu, Japan). Concentration of MB in the solution was determined as a function of irradiation time from absorbance change at the wavelength of 664 nm, using the calibration curve determined in advance. Since the plots of logarithm of relative concentration of MB in the solution $\ln(C/C_0)$ against irradiation time were approximated to be linear, the slope of the linear relation, i.e., rate constant k, was determined on each sample and used as a measure of the photocatalytic activity of the sample.

3. Results and discussion

3.1 XRD analysis

Fig. 1(a) shows the XRD pattern of pure TiO_2. The XRD pattern shows the presence of the peaks at 2θ=25.4˚, 38.0˚, 48.1˚, 54.2˚, and 62.4˚, regarded as an attributive indication of anatase TiO_2, which is coincided with standard JCPDS card (PDF # 21-1272). The peaks are indexed as (101), (112), (200), (211) and (204) in the order of

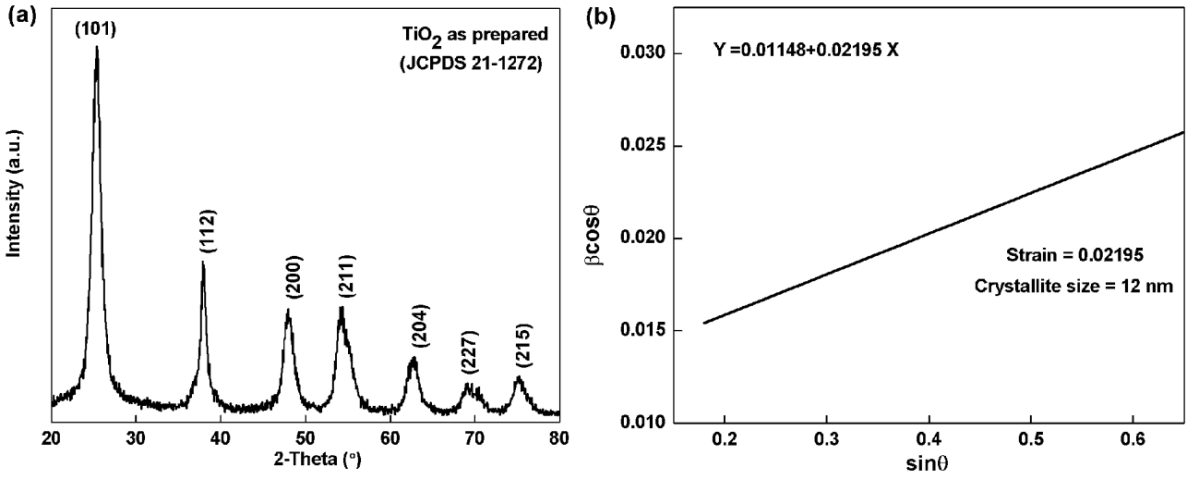

Fig. 1. (a) XRD pattern; (b) W-H plot of pure TiO_2.

increasing diffraction angles, respectively. The XRD results indicate that the as-synthesized TiO_2 powder has been predominantly crystallized into anatase phase. The values of strain and average crystallite sizes are estimated from

Williamson-Hall plot using X-ray peak broadening (Venkateswarlu et al., 2010). The plot between sinθ and βcosθ is shown in Fig. 1(b). The strain is estimated from the slope of the line which is 0.02195, and the crystallite size 'd' can be calculated from the intersection of the line with y-axis which is 12 nm. Fig. 2 shows the XRD pattern of as-synthesis Ag-TiO_2 and 500 ˚C annealed samples. The presence of anatase phase without any impurity phases such as, Ag or $AgNO_3$ confirms the complete doping of Ag in TiO_2 matrix. Also, it is inferred that the formed anatase phase is stable even at 500 ˚C. The average crystallite size 'd' is estimated from the broadening of XRD peaks using Scherrer equation from Eq. (1). The highest intensity peak (101) is used to calculate the crystallite size 'd' of the samples. The crystallite size for Ag-TiO_2 in as-synthesis condition and in 500 ˚C annealed condition is found to be 7 nm and 9 nm, respectively.

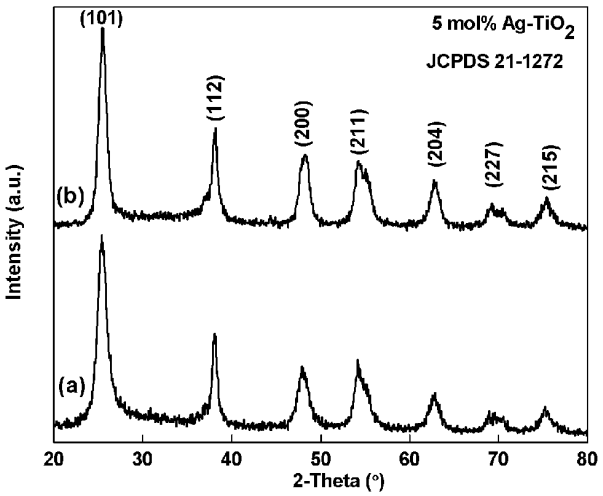

Fig. 2. XRD pattern of Ag-TiO_2 (5 mol%) in (a) as-synthesis; (b) annealed at 500 ˚C.

3.2 UV-Vis spectroscopy

It is well known that different materials absorb radiation of different wavelengths and the yield of photo generated electron-hole pair depends primarily on the intensity of incident photons with energy exceeding or equaling the TiO_2 band gap energy. Fig. 3(a) shows the UV-Vis spectra of pure TiO_2 and Ag-TiO_2 samples. It is shown from Fig. 3(a) that compared to pure TiO_2, the absorption edge shifts towards longer wavelengths for Ag-TiO_2 sample. This shift in absorption edge for Ag-TiO_2 is due to the introduction of the impurity levels with Ag doping. The optical band gap energy E_g was determined by using the Tauc equation (Peiqiang et al., 2014) by plotting $(\alpha h\nu)^{1/2}$ versus photon energy ($h\nu$) and extrapolating the linear portion to $(\alpha h\nu)^{1/2} = 0$;

$$\alpha = \mathrm{K}\frac{\left(h\upsilon - E_g\right)^2}{h\upsilon} \tag{3}$$

where, K is constant, $h\nu$ is the photon energy and E_g is the band gap energy for indirect transitions. The absorption co-efficient (α) can be calculated from the measured absorbance (A) using the following equation;

$$\alpha = \frac{2.303\rho 1000}{lCM}A \tag{4}$$

where, the density ρ = 3.9 g.cm^{-3}, molecular weight M=79.9 g/mol, C = molar concentration of TiO_2 and l is the optical path length. The plots of $(\alpha h\nu)^{1/2}$ versus $h\nu$ for pure TiO_2 and Ag-TiO_2 are shown in Fig. 3(b). The intersection of the extrapolated linear portions gives the band gap energy (E_g). The linear nature of the plots above the absorption edge indicates that the fundamental optical transition in these materials is indirect. The estimated

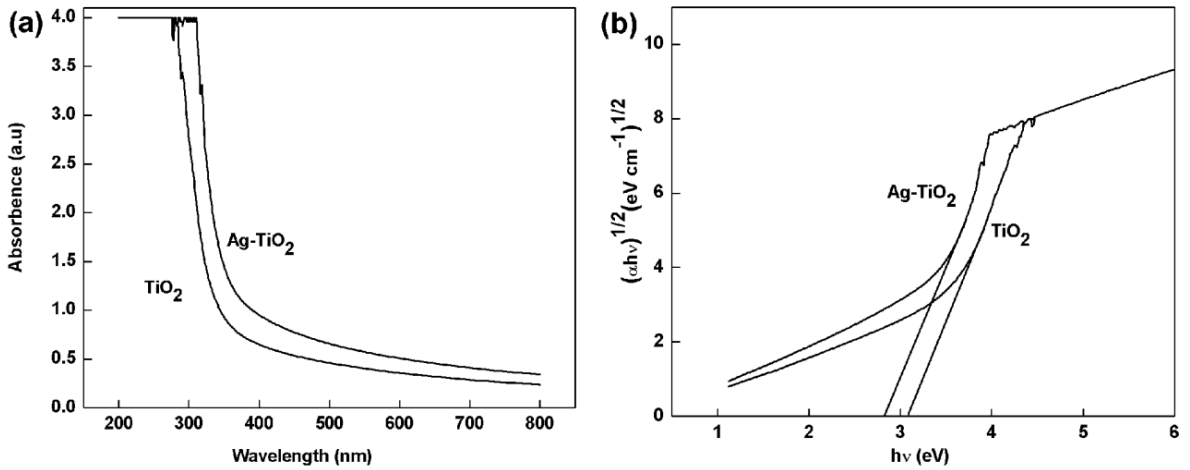

Fig. 3. (a) UV-Vis absorption spectra; (b) plot of $\alpha^{1/2}$ versus E_{phot} for indirect transition of TiO_2 and Ag-TiO_2 samples. Band gap energy E_g is obtained by extrapolation to α=0.

band gap energy for pure TiO_2 is found to be 3.10 eV and for Ag-TiO_2, band gap energy is 2.90 eV. The result shows that 5 mol% Ag doping extends the absorbance spectrum of TiO_2 to longer wavelengths and reduced the band gap from 3.10 eV to 2.90 eV.

3.3 Antibacterial ability

The bactericidal activity of TiO_2 and Ag-TiO_2 was studied by spread plate method. The spread plate result of Ag-TiO_2 sample with 1×10^5 cells/mL of *Escherichia coli* were examined after 24 hours. For comparison, pure TiO_2 sample was also tested and the images are presented in Fig. 4. The results reveal that, Ag-TiO_2 sample shows complete inhibition of the bacterial growth under the present incubation condition of 24 h (Fig. 4), whereas, pure

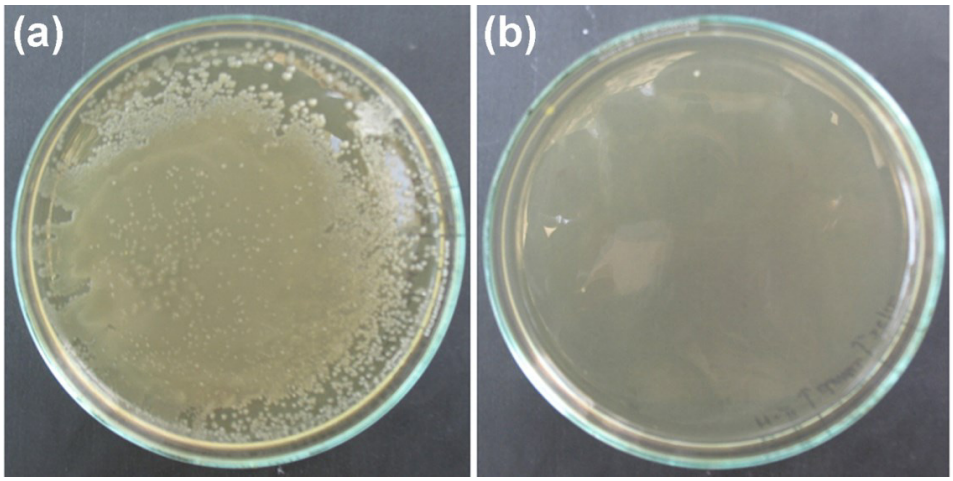

Fig. 4. Spread plate results of (a) pure TiO_2 (b) Ag-TiO_2 samples after 24 h with 1x 10^5 cells/mL of *Escherichia coli*.

TiO_2 sample shows the presence of bacterial colonies. The enhancement of antibacterial property of Ag-TiO_2 compared to pure TiO_2 is mainly due to the following reason. When Ag-TiO_2 particles are dispersed in the growth

media, the Ag atoms present in these particles interact with the bacterial cells and adhere to the bacterial cell walls. The electrostatic forces between bacteria and Ag atoms may be the reason for their adhesion. Due to the excess number of carboxylic and other groups, the overall charge on the bacterial cell surface at biological pH values is negative (Thiel et al., 2007). Further, Djokic and Burrel (1998) reported that ionic Ag strongly interacts with thiol groups of vital enzymes and inactivates them and once treated with Ag ions the DNA loses its replication ability which results in cell death. Thus in our present study, the presence of Ag in TiO_2 significantly enhanced the antibacterial property of TiO_2.

3.4 Photocatalytic assessment

The photocatalytic activity of TiO_2 and Ag-TiO_2 nanopowders was studied by the degradation of MB aqueous solution under UV light irradiation. Fig. 5(a) shows the variation of MB (10 ppm) degradation with TiO_2 at different annealing temperatures and at a fixed catalyst amount of 1.5 g/L. The highest photocatalytic degradation is observed for the sample annealed at 500 ˚C. Comparing with as-prepared TiO_2, TiO_2 annealed at 500 ˚C possesses excellent crystallinity. Further, the photocatalytic activity is slightly reduced when the sample is annealed at 800 ˚C. According to Ohtani et al., the high activity of TiO_2 photo catalyst should satisfy two requirements (Ohtani et al., 1997): large surface area for absorbing dye and high crystallinity to reduce photo-excited electron-hole recombination rate. In general, the crystallinity increases with annealing temperature, while the surface area decreases with temperature. In addition, annealing increases the crystallinity of TiO_2, thereby decrease in the content of amorphous TiO_2 and depress the photo excited electron-hole recombination; and thus increase in the photocatalytic activity. However annealing at very high temperatures increases the particle size and decreases the surface area and favors the phase transformation from anatase to rutile. Hence, an optimum annealing temperature is to be chosen to avoid these undesirable affects. Thus, TiO_2 sample annealed at 500 ˚C having high crystallinity (Fig. 1(a)) showed higher degradation rate of MB in the present study.

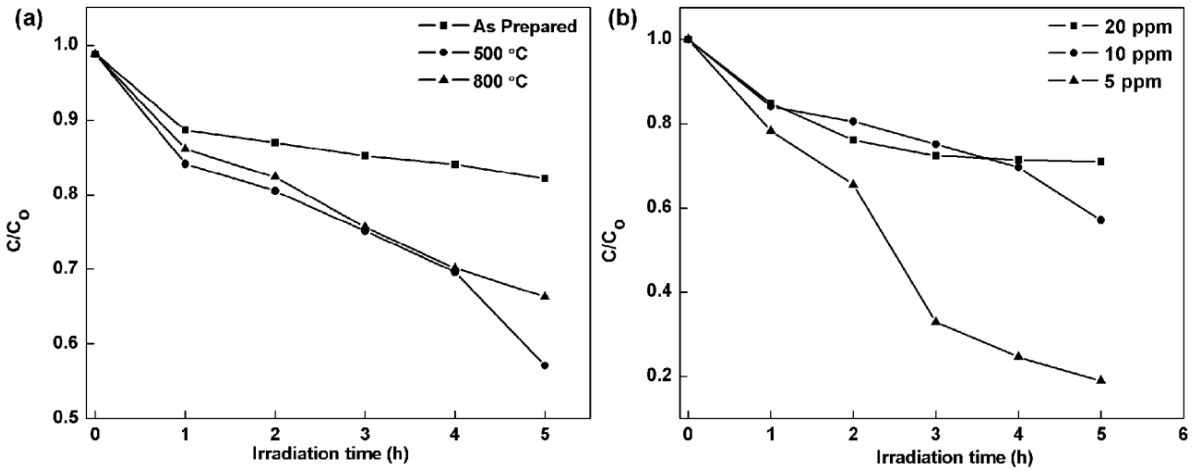

Fig. 5. (a) Photocatalytic activity of TiO_2 sample as-synthesized and annealed at different temperatures towards MB (10 ppm) under UV-light radiation with increasing irradiation time; (b) Effect of MB concentration on photo degradation rate of TiO_2 sample annealed at 500 ˚C (catalyst dosage 1.5 g/L).

Fig. 5(b) shows the effect of concentration of MB at a fixed catalyst amount (1.5 g/L) on the percentage of degradation of MB with 500 ˚C annealed TiO_2 under UV radiation. It is found that with an increase in the dye concentration from 5 ppm to 20 ppm, the degradation of MB decreases from 81% to 33%. The degradation efficiency is higher for lower MB concentration. At higher concentration of the dye, the light absorbed by the dye is more than that of the catalyst, and the light absorbed by the dye is not effective for the photocatalytic degradation. For a fixed catalyst dose, the active sites remaining the same, however, the number of dye ions accommodated in the

interlayer space increases and hence catalyst surface becomes saturated with the same number of dye ions. So, there is a decrease in percentage of degradation on the dye.

In order to study the photocatalytic activity of Ag-TiO_2, the MB degradation is studied with 5 ppm concentration and catalyst amount as 1.5 g/L and the obtained results are compared with pure TiO_2. From Fig. 6(a), it is observed that the % degradation increases with UV exposure time and the photocatalytic activity is improved with Ag doping in TiO_2. Pure TiO_2 shows 81% degradation on MB after 5 hours of UV exposure, whereas, Ag-TiO_2 sample shows 88% degradation for the same exposure time. The apparent rate constant has been chosen as the basic kinetic parameter for the different photo catalysts, since it enables to determine a photocatalytic activity independent of the previous adsorption period in the dark and the concentration of MB remaining in the solution. The apparent first-order kinetic equation $\ln(C_o/C) = k_{app}$ is used to fit experimental data, where k_{app} is apparent rate constant, C is the solution-phase concentration of MB and C_o is the initial concentration at t=0 (Matos et al., 1998). The variations in $\ln (C_o/C)$ as a function of irradiation time are given in Fig. 6(b). The apparent rate constants k_{app} is found to be 0.31 and 0.49 h^{-1} for pure TiO_2 and Ag-TiO_2 samples, respectively.

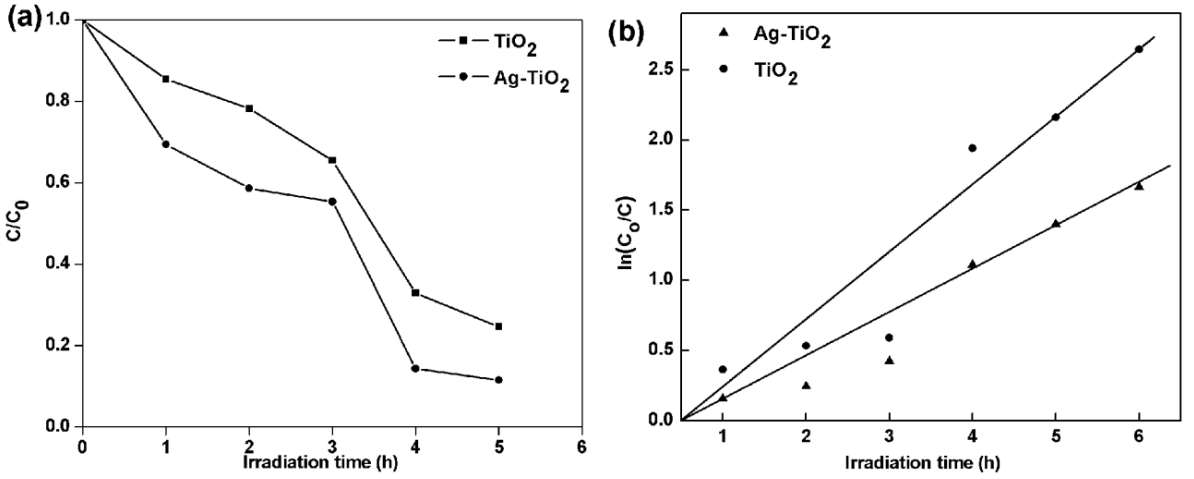

Fig. 6. (a) Effect of Ag doping on MB photo degradation (catalyst dosage 1.5 g/L, 5 ppm) and (b) Linear transformation $\ln(C_0/C)=f(t)$ of the kinetic curves of MB disappearance for TiO_2 and Ag-TiO_2 samples.

When a photon of UV light strikes the surface of TiO_2, a valence band electron moves to the conduction band, thus forming a positively charged hole in the valence band. These holes and electrons generate reactive oxygen species such as O_2^- and OH^- radicals, which attack dye molecules and lead to their degradation. The enhancement of MB degradation for Ag-TiO_2 may be due to its ability to trap electrons (Subbarao et al., 2003). This process reduces the recombination of charges and favors oxidation of dye. The reduction potential of Ag ion is suitably positioned for the effective photocatalytic reduction producing metallic Ag^+ on TiO_2 surface. This is further evidenced by the slight color change of the catalyst into black. Thus, the presence of 5 mol% Ag significantly enhanced the photocatalytic activity of TiO_2.

4. Conclusions

Nanostructured pure TiO_2 and Ag doped TiO_2 powders were synthesized successfully by sol-gel method using titanium tetra n-butoxide as titanium precursor. XRD spectra confirmed the presence of anatase phase in both TiO_2 and Ag-TiO_2 samples with crystallite size varying from 6-15 nm. The crystallize size and crystallinity of both the samples were increased with annealing temperature. The UV-Vis studies showed the shift in the absorbance towards

longer wavelengths for Ag doped TiO_2. The band gap was found to be 3.1 eV for pure TiO_2 and 2.9 eV for Ag-TiO_2. The antibacterial activity of pure TiO_2 and Ag-TiO_2 is assessed by spread plate method against 10^5 cells/mL of *Escherichia coli* bacteria after an incubation period of 24 h. Bacterial colonies were not observed in Ag-TiO_2 treated plates whereas, numerous bacterial colonies were observed in TiO_2 treated plates. Photocatalytic activity of both TiO_2 and Ag-TiO_2 samples was examined by decomposition of MB for 5 h under UV irradiation. It is found that the photocatalytic degradation depends on the catalyst crystallinity and dye concentration. The MB degradation is higher for the TiO_2 sample annealed at 500 ˚C compared to as-synthesized TiO_2. Further, the degradation is more for lower concentrations of the dye and it decreases with increase in the dye concentration. The photocatalytic degradation is higher for Ag-TiO_2 compared to pure TiO_2 samples and the photocatalytic inactivation of MB in presence of UV irradiation was observed to follow first order kinetics. This improved photocatalytic activity of Ag-TiO_2 samples may be due to a decrease in the recombination rate of photo generated charge carriers and decrease in the band gap from 3.1 eV to 2.9 eV.

References

Brinker, C.J., Scherrer, G.W., 1990. Sol-gel Science: The Physics and Chemistry of Sol-Gel Processing, fifth ed., Academic press, New York.

Carp, O., Huisman, C.L., Reller, A., 2004. Photo Induced Reactivity of Titanium Dioxide. Progress in Solid State Chemistry 32, 33-177.

Chen, X., Mao, S.S., 2007. Titanium Dioxide Nanomaterials: Synthesis, Properties, Modifications and Applications. Chemical Reviews 107, 2891-2959.

Diebold, U., 2003. Structure and Properties of TiO_2 Surfaces: A Brief Review. Applied Physics A: Materials Science and Processing 76, 681-687.

Ding, X.Z., Liu, X.H., 1997. Synthesis and Microstructure Control of Nanocrystalline Titania Powders via a Sol-Gel Process. Materials Science and Engineering A 224, 210-215.

Diwald, O., Thompson, T.L., Zubkov, T., Goralski, E.G., Walck, S.D., Yates, J.T., 2004. Photochemical Activity of Nitrogen-Doped Rutile TiO_2 (110) in Visible Light, The Journal of Physical Chemistry B 108, 6004-6008.

Djokic, S.S., Burrel, R.E., 1998. Behavior of Silver in Physiological Solutions. Journal of the Electrochemical Society 145, 1426-1430.

Dulce. J.R.G., Nini, R.M., Susana, S.M., 2013. Photocatalytic activity enhancement of TiO_2 thin films with silver doping under visible light. Journal of Photochemistry and Photobiology A: Chemistry 262, 57-63.

Feng, Q.L., Wu, J., Chen, G.Q., Cui, F.Z., Kim, T.N., Kim. J.O., 2000. A Mechanistic Study of the Antibacterial Effect of Silver Ions on *Escherichia Coli* and Staphylococcus Aureus. Journal of Biomedical Materials Research Part 52, 662-668.

Fujishima, A., Rao, TN., Tryk, D.A., 2000. Titanium dioxide photocatalysis. Journal of Photochemistry and Photobiology C: Photochemistry Reviews 1, 1-21.

Fujishima, A., Zhang, X, 2006.Titanium Dioxide Photocatalysis: Present Situation and Future Approaches. Comptes Rendus Chimie 9, 750-760.

Gonzalez, J.S., Maiolo, A.S., Hoppe, C.E., Alvarez, V.A., 2012. Composite Gels Based on Poly (vinyl alcohol) for biomedical uses. Procedia Materials Science 1, 483-490.

He, C., Yu, Y., Hu, X., Larbot, A., 2002. Influence of Silver Doping on the Photocatalytic Activity of Titania Films. Applied Surface Science 200, 239-247.

Klug, H.P., Alexander, L.E., 1954. X-Ray Diffraction Procedures: for Polycrystalline and Amorphous Materials, second ed., John Wiley & Sons, New York.

Koch, C.C., 2006. Nanostructured Materials: Processing, Properties and Potential Applications, second ed., Noyes publications, New York.

Maness, P.C., Smolinski, S., Blake, D.M., Huang, Z., Wolfrum, E.J., Jacoby, W.A., 1999. Bactericidal activity of photocatalytic TiO_2 reaction : Toward an Understanding of Its Killing Mechanism. Applied and Environmental Microbiology 65, 4094-4098.

Matos, J., Laine, J., Herrmann, J.M., 1998. Synergy Effect in the Photocatalytic Degradation of Phenol on a Suspended Mixture of Titania and Activated Carbon. Applied Catalysis B: Environmental 18, 281-291.

Mohammadi, M.R., Fray, D.J., Mohammadi, A., 2008. Sol-gel Nanostructured Titanium Dioxide: Controlling the Crystal Structure, Crystallite Size, Phase Transformation, Packing and Ordering. Microporous Mesoporous Materials 112, 392-402.

Morones, J.R., Elechiguerra, J.L., Camacho, A., Holt, K., Kouri, J.B., Ramírez, J.T., Yacaman, M.J., 2005. The Bactericidal Effect of Silver Nanoparticles. Nanotechnology 16, 2346-2353.

Mukhtar, H.A., Tia, E.K., John, A.B., Charles, W.B., Jeremy, W.H., 2011. Adsorption and photocatalytic degradation of human serum albumin on TiO_2 and Ag-TiO_2 films. Journal of Photochemistry and Photobiology A: Chemistry 222, 123-131.

Nosaka, Y., Matsushita, M., Nishino, J., Nosaka, A.Y., 2005. Nitrogen-Doped Titanium Dioxide Photocatalysts for Visible Response Prepared by Using Organic Compounds. Science and Technology of Advanced Materials 6, 143-148.

Ohtani, B., Ogawa, Y., Nishimoto, S.I., 1997. Photocatalytic Activity of Amorphous-Anatase Mixture of Titanium (IV) Oxide Particles Suspended in Aqueous Solutions. The Journal of Physical Chemistry B 101, 3746-3752.

Peiqiang, L., Haitao, H., Jinfeng, X., Hua, J., Hui, P., Jing, L., Chenxiao, W., Shiyun, A., 2014. New Insights into the Photo-enhanced Electro catalytic reduction of carbon dioxide on MoS2-rods/TiO2 NTs with unmatched energy band. Applied Catalysis B: Environmental 147, 912-919.

Quan, X., Huaiqin, T., Qinghua, Z., Xuemei, S., 2007. Preparation of Lanthanum-Doped TiO_2 Photocatalysts by Coprecipitation, Journal of Materials Science 42, 6287-6296.

Ramya, S., Nithila, S.D.R., George, R.P., Gopalakrishna, D.N., Thinaharan, C., Kamachimudali, U., 2013. Antibacterial studies on Eu-Ag codoped TiO_2 surfaces. Ceramics International 39, 1695-1705.

Rodríguez, J.A., Fernández-García, M., 2007. Synthesis, Properties and Applications of Oxide Nanomaterials. John Wiley & sons, New Jersey.

Sandhyarani, M., Rameshbabu, N., Venkateswarlu, K., Ravisankar, K.V., Ashok, M., Anandan, S., 2013. Photocatalytic and Antibacterial Activity of Titanium, Fluorine and Silver Co-substituted Hydroxyapatite. International Journal of Modern Physics: Conference Series 22, 268-277.

Seery, M.K., George, R., Floris, P., Pillai, S.C., 2007. Silver Doped Titanium Dioxide Nanomaterials for Enhanced Visible Light Photocatalysis. Journal of Photochemistry and Photobilogy A: Chemistry 189, 258-263.

Sharad, S., Mohan, C., Giridhar, M., 2012. Visible light photocatalytic inactivation of *Escherichia coli* with combustion synthesized TiO_2. Chemical Engineering Journal 189-190, 101-107.

Subba Rao, K.V., Lavedrine, B., Boule, P., 2003. Influence of Metallic Species on TiO_2 for Photocatalytic Degradation of Dyes and Dye Intermediates. Journal of Photochemistry and Photobiology A: Chemistry 154, 189-193.

Thiel, J., Pakstis, L., Buzby, S., Raffi, M., Ni, C., Pochan, D.J., Shah, S.I., 2007. Antibacterial Properties of Silver-Doped Titania. Small 3, 799-803.

Venkateswarlu, K., Chandrabose, A., Rameshbabu, N., 2010. X-ray Peak Broadening Studies of Nanocrystalline Hydroxyapatite by Williamson Hall Analysis. 405(20) 4256-4261.

Wang, G., 2007.Hydrothermal Synthesis and Photocatalytic Activity of Nanocrystalline TiO_2 Powders in Ethanol-Water Mixed Solutions. Journal of Molecular Catalysis A: Chemical 274, 185-191.

Wilke, K., Breuer, H.D., 1999. The Influence of Transition Metal Doping on the Physical and Photocatalytic Properties of Titania. Journal of Photochemistry and Photobiology A: Chemistry 121, 49-53.

Wilson, M., Kanagara, K., Smith, G., Simmons, M., Raguse, B., 2002. Nano Technology: Basic Sciences and Engineering Technologies. CRC Press, USA.

Yin, S., Zhang, Q., Saito, F., Sato, T., 2003. Preparation of Visible Light-Activated Titania Photocatalyst by Mechanochemical Method. Chemistry Letters 32, 358-359.